International Journal of Applied Earth Observations and Geoinformation 103 (2021) 102478

Contents lists available at ScienceDirect

International Journal of Applied Earth Observations and Geoinformation

journal homepage: www.elsevier.com/locate/jag

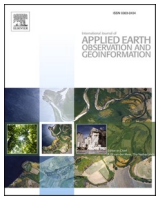

Estimating fine-scale visibility in a temperate forest landscape using airborne laser scanning

Xin Zong [a,*], Tiejun Wang [a], Andrew K. Skidmore [a,b], Marco Heurich [c,d,e]

[a] Faculty of Geo-Information Science and Earth Observation (ITC), University of Twente, Enschede, the Netherlands
[b] Department of Environmental Science, Macquarie University, Sydney, Australia
[c] Department of Conservation and Research, Bavarian Forest National Park, Grafenau, Germany
[d] Chair of Wildlife Ecology and Management, University of Freiburg, Freiburg, Germany
[e] Institute for Forestry and Wildlife Management, Inland Norway University of Applied Science, Koppang, Norway

ARTICLE INFO

Keywords:
Viewshed
Airborne LiDAR
Terrestrial LiDAR
Understory
Random forests

ABSTRACT

Visibility is a key factor influencing animal behavior in forest ecosystems. Fine-scale visibility in forested areas has been measured by ground-based approaches at the plot level, using site-specific methods that have limited spatial coverage. Here we examine airborne laser scanning (ALS) as a novel tool to quantify fine-scale visibility in the temperate forests of Germany at a landscape scale. We validate the (vertically-derived) ALS-derived visibility measures using proven (horizontally-derived) terrestrial laser scanning (TLS) estimates of true visibility. Our results indicate that there is a good agreement between the visibility resulting from ALS and TLS with an R^2 ranging from 0.53 to 0.84 and a normalized RMSE varying from 15.92% to 11.81% at various plot sizes, with the highest accuracy achieved using a plot size of 35 × 35 m. Our study demonstrates for the first time that ALS can be successfully applied to quantify fine-scale visibility in temperate forests at a landscape level. This approach holds potential for studying the spatial behavior of animals (*e.g.*, habitat selection and predator–prey relationships) in forest ecosystems.

1. Introduction

Visibility (viewshed) analysis has been applied to a range of applications in forest ecosystems, from locating fire watchtowers (Bao et al., 2015; Göltaş et al., 2017), hiding scars from timber harvest (Chamberlain et al., 2015; Domingo-Santos et al., 2011), planning military operations (Caldwell et al., 2005; Drummond, 1956), to studying animal spatial behavior (Dupke et al., 2017; Loarie et al., 2013). However, despite the successful application of visibility analysis in natural resource management, previous studies indicate that measurement of fine-scale visibility in forest environments, particularly at the landscape level, is a challenge considering the architectural complexity of the plant (Murgoitio et al., 2014) which causes objects such as animals to be obscured (camouflaged) by vegetation.

Visibility analysis is typically performed by checking whether the components block the sightline between an observer and a target in the modeled environmental scene. The level of complexity and precision of depicting an environmental scene depends on the goal and scale of the application (Vukomanovic et al., 2018). Environmental factors such as topographic and manmade features all influence the visibility of the surrounding area across spatial scales. Particularly in the case of forests, vegetation representation has a significant impact on perceived visibility. For landscape-scale (*e.g.*, several square kilometers) applications that assess the influence of coarse features on visibility, vegetation is typically treated as digital surface models, as implemented in most geographic information systems (GIS) (Loarie et al., 2013; Vukomanovic et al., 2018). For certain applications, such as research on animal ecology and military goals, fine-scale visibility should be estimated at distances ranging from several to tens of meters when the view is often lateral and under the canopy. Within very short ranges, and particularly in areas of high vegetation density, visual obstruction is frequently dominated by the fine-scale 3D plant structure in the understory including trunks, branches, leaves, and internal gaps. In this regard, for these short-range applications, fine-scale visibility in forests often refers to fine-scale visibility in the understory (Murgoitio et al., 2014). The digital surface model used for landscape-scale applications is not

* Corresponding author.
E-mail addresses: x.zong@utwente.nl (X. Zong), t.wang@utwente.nl (T. Wang), a.k.skidmore@utwente.nl (A.K. Skidmore), marco.heurich@npv-bw.bayern.de (M. Heurich).

https://doi.org/10.1016/j.jag.2021.102478
Received 26 April 2021; Received in revised form 17 July 2021; Accepted 3 August 2021
Available online 11 August 2021

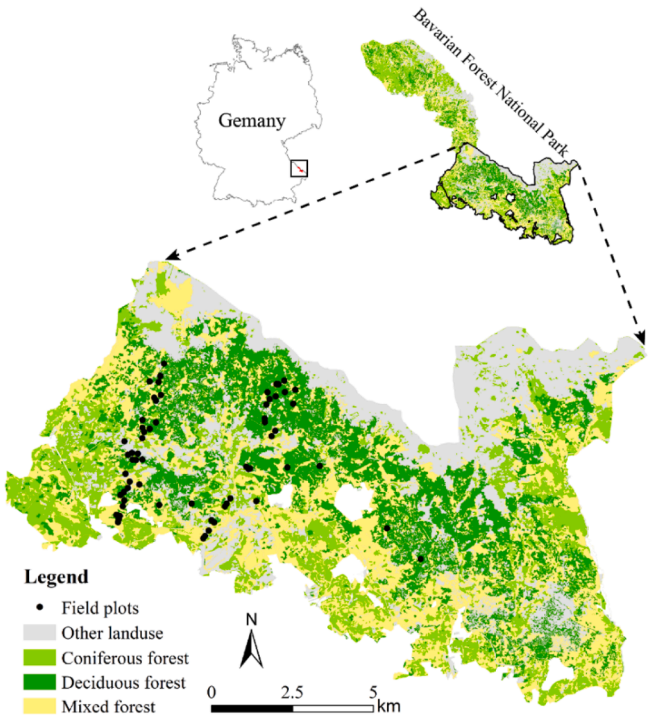

Fig. 1. Location of field plots in the southern part of the Bavarian Forest National Park, Germany.

suitable for assessing fine-scale visibility in forests, as it does not contain understory information. As such, visibility analysis functions in GIS have not been adopted by short-range applications in forests.

Fine-scale visibility in forests is typically measured in the field by observing or photographing a remote reference object of known size from a given viewpoint, and therefore determining the percentage of an object covered by vegetation (Higgins et al., 1996). The two most commonly used reference objects are a cover board or a pole (Griffith and Youtie, 1988; Winnard et al., 2013). The proportion of vegetation obstruction is nearly always determined through visual interpretation on the ground or by the automatic classification of photographs (Campbell et al., 2018; Morrison, 2016). However, one of the major limitations of these classical approaches is that visibility will only be obtained from a predetermined viewpoint and in limited directions, often four or eight cardinal directions. Moreover, the sampling efficiency is low and measurements are hard to replicate.

Terrestrial laser scanning (TLS) can generate highly dense laser returns especially in the lower vegetation layers (*e.g.*, canopy base, understory, and terrain) and thereby capture the 3D structure at a fine spatial resolution (<2 cm), which allows representing the 3D structure of forest stands with substantial details (Dassot et al., 2011). Thanks to these advantages of TLS, it has recently started to be applied to quantify fine-scale visibility in forests in some studies. For example, Lecigne et al. (2020) developed an R package "viewshed3d" to generate 3D viewshed by tracing cone-shaped sightlines within the TLS point cloud in every direction of 3D space to determine their traveling distances before they meet any TLS point. Zong et al. (2021) proposed to build a 3D voxel model of the surrounding scene with TLS data using the occupancy grid algorithm and then trace the sightlines within the voxel model. In contrast, the sightline was treated as a straight line rather than a cone. Compared to traditional field methods, TLS may estimate visibility at any location and from any direction across a continuum of scales in a scanned area, and can therefore generate a 3D viewshed which refers to the volume in a 3D environment that is directly visible from a vantage position, in a similar way as the viewshed on the digital elevation model (DEM) (Wheatley, 1995). Moreover, a 3D cumulative viewshed of the scanned area can be created by computing repeatedly 3D viewsheds from several pre-defined viewpoints and then summing them up into a single 3D viewshed (Lecigne et al., 2020). TLS has proven to be an effective and efficient method to estimate 3D detailed visibility. However, the TLS-derived estimate of fine-scale visibility is ground-based at plot level, and is therefore site-specific with limited spatial coverage. For a more extensive assessment of detailed visibility at larger spatial scales, these measurements would need to be repeated in many locations. So it is not practical to continuously characterize detailed visibility in a landscape using such an approach.

Compared to TLS, airborne laser scanning (ALS) can provide insight into forest structure in larger areas. Currently, ALS has mainly been used to generate upper canopy surface models for visibility analysis in forested areas (Guth, 2009; Vukomanovic et al., 2018). However, the ability of ALS to quantify fine-scale visibility in understory on a large scale remains rather unexplored. Only three studies have investigated the utility of ALS in modeling the visual obstruction arising from vegetation below the canopy. Murgoitio et al. (2013) used the diameter at breast height and tree height to account for the visual obstructions of tree trunks in the visibility model, but ignored the branches and leaves. Murgoitio et al. (2014) also examined the correlation between canopy area and the number of trunks derived from ALS data and the visibility of forest plots derived from TLS and the photography-based method respectively and found a relatively low association. Additionally, the visibility investigated in these studies was confined in several predefined directions and limited at the plot scale. Pyysalo et al. (2009) performed a visibility analysis on a 3D voxel model of the forest environment with a voxel size of 1 m built from ALS data. However, the voxel size was not fine enough to quantify detailed visibility. Moreover, they have not evaluated the accuracy of their approach.

So far, there have been no suitable methods for characterizing fine-scale visibility in forests across landscapes, which severely limits the use of visibility in short-range applications. The visibility measured by both conventional field methods and the single 3D viewshed obtained by TLS is viewpoint specific. The visibility of the same area obtained at different viewpoints may be highly varied due to the spatial heterogeneity of the vegetation structure. Therefore, extrapolation of the estimated visibility of these two methods to other areas is difficult. By contrast, a 3D cumulative viewshed derived from the TLS arises from the integration of 3D viewsheds from multiple viewpoints, thereby comprehensively quantifying the relative visibility of an area of interest in a landscape. Similar to the characterization of other understory structure attributes using the area-based approach of Næsset (2002), the area-based cumulative visibility can be statistically linked to ALS-derived metrics within that same area. ALS is likely a viable way to upscale the TLS-based cumulative visibility at the plot level to the landscape scale "wall-to-wall" spatial coverage.

Our study is designed to assess the capacity of ALS data to characterize fine-scale visibility in mixed temperate forests at the landscape scale, by calibrating and validating the ALS visibility model using TLS-based cumulative visibility estimates at the plot level. Specifically, we sought to: (1) evaluate the performance of 23 frequently used ALS metrics to quantify fine-scale visibility and select important input metrics at multiple plot sizes respectively, (2) identify the most important ALS metrics for quantification of fine-scale visibility, and (3) determine the optimal plot size for upscaling fine-scale visibility derived from TLS to a landscape scale using ALS.

2. Material and methods

2.1. Study site

The study site lies in the southern part of the Bavarian Forest National Park, a mixed temperate forest located in southeastern Germany (49°3′19″N, 13°12′9″E) (Fig. 1). The park extends over an area of 24,250 ha with altitudes between 590 and 1440 m. The predominant

Table 1
TLS data specifications.

Specification	Value
Sensor	RIEGL VZ-400
Wavelength	1550 nm
Beam divergence	0.35 mrad
Scan angle	Horizontal: 360° Vertical:100° (+60°/−40°)
Measurement rate	122,000 measurements/second
Range accuracy	5 mm
Range	1.5–600 m

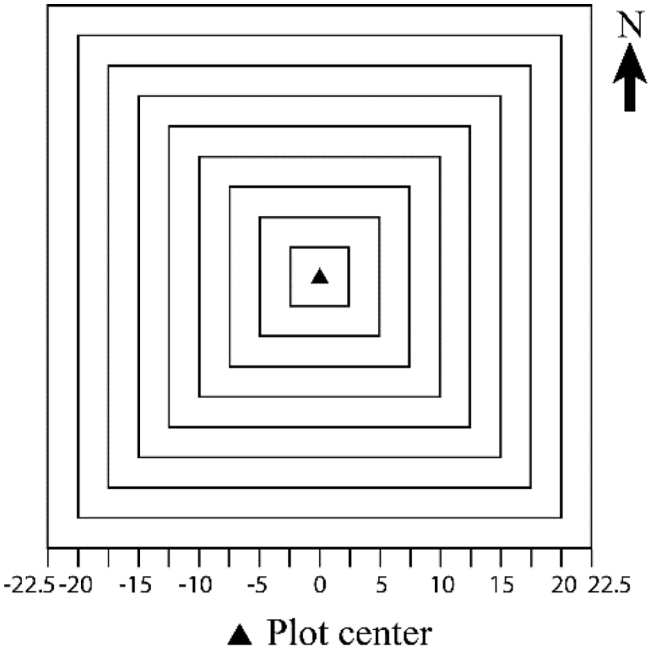

Fig. 2. The size, position, and orientation of the square plots for estimation of visibility using TLS.

tree species of the park are Norway spruce (*Picea abies*) (67%) and European beech (*Fagus sylvatica*) (24.5%) (Cailleret et al., 2014).

2.2. TLS data

TLS data were collected during the summer (July or August) of 2016, 2017, and 2019, respectively, using a time-of-flight scanner RIEGL VZ-400 (Riegl LMS GmbH, Horn, Austria) (Table 1). A total of 66 sample plots were gathered, each with a radius of 22.5 m. The plot centers were geo-located using a Leica Viva GS14 differential GNSS receiver with a spatial accuracy of around 5–10 cm. The plots represent three types of forests (*i.e.*, coniferous, deciduous, and mixed) and three categories of stand developmental stages (*i.e.*, young, medium, and mature). To minimize occlusion, four scans were acquired at each plot, with one scan at the plot center, three at the edge of the plot. To co-register these four scans, 12–14 cylindrical *retro*-reflective targets were placed in the plot to serve as control points.

Table 2
Description of ALS metrics used as predictor variables for modeling visibility.

Metrics		Description
Canopy	Hp10_can	10th height percentiles of canopy returns
	Hp50_can	50th height percentiles of canopy returns
	Hp70_can	70th height percentiles of canopy returns
	Hp90_can	90th height percentiles of canopy returns
	Hsd_can	Standard deviation of canopy return heights
	Hskew_can	Skewness of canopy return heights
	Hkurt_can	Kurtosis of canopy return heights
	P_ground	Percentage of ground returns
Understory	Hp10_us	10th height percentiles of understory returns
	Hp50_us	50th height percentiles of understory returns
	Hp70_us	70th height percentiles of understory returns
	Hp90_us	90th height percentiles of understory returns
	ORD	Overall relative point density
	NRD	Normalized relative point density
	LPI	Laser penetration index
	P_NRD	Percentage of NRD
	P_LPI	Percentage of LPI
	Hp99_sd	Standard deviation of 99th height percentiles of understory returns
	Hp99_cv	Coefficient of variation of 99th height percentiles of understory returns
	NFC	Number of filled columns
	NFV	Number of filled voxels
Topography	VRM	Vector ruggedness measures
	TRI	Terrain ruggedness index

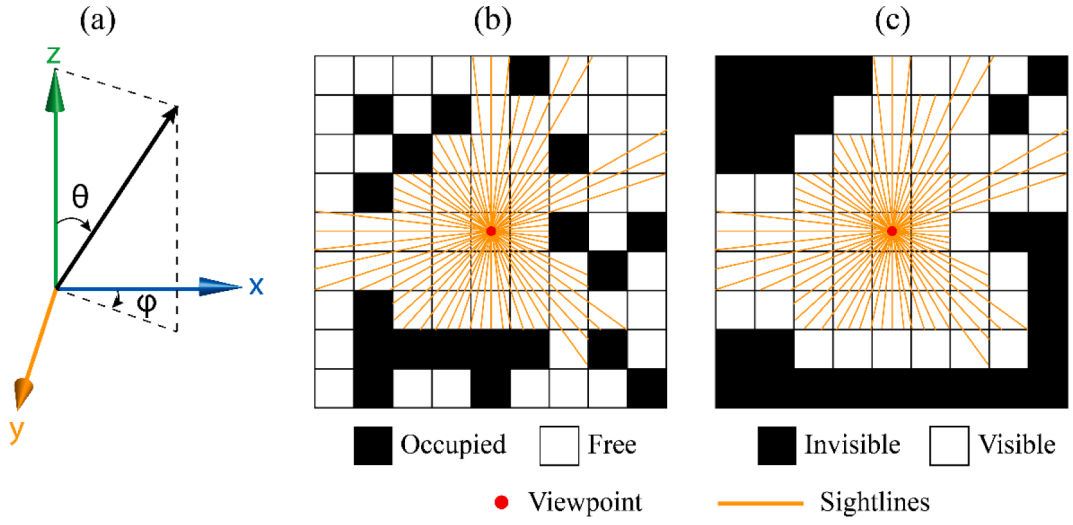

Fig. 3. Illustration of the process of calculating 3D viewshed: (a) a sightline with an azimuth angle of φ and a zenith angle of θ; (b) 2D representation of tracing sightlines within the occupancy grid model; and (c) 2D representation of the generated viewshed.

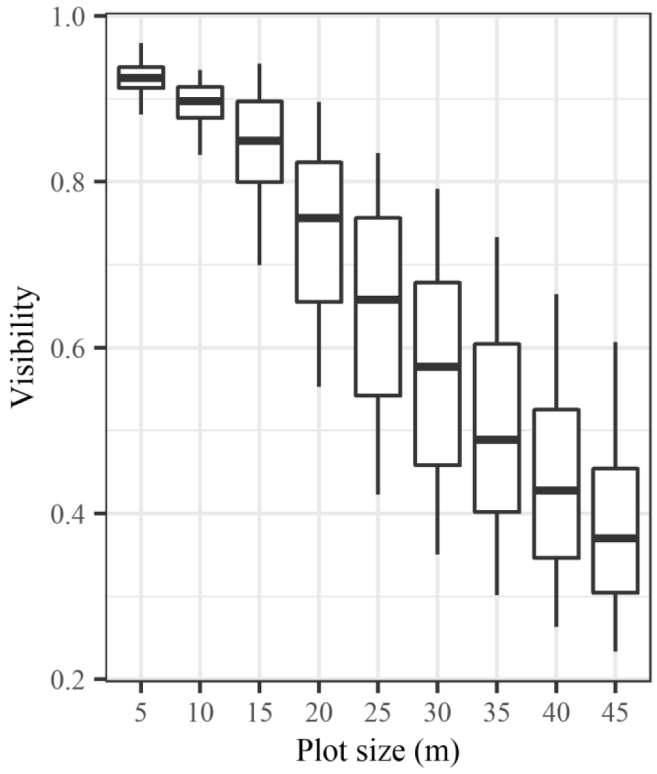

Fig. 4. Box and whiskers representing TLS-derived visibility of the plots at different plot sizes.

We classified TLS ground points using the LAStools software package (version 171017, rapidlasso GmbH, http://lastools.org) and generated digital terrain models (DTM) with a resolution of 0.2 m. The height of each above-ground TLS return was normalized by subtracting the elevation of the DTM.

2.3. ALS data

The ALS flight campaign was conducted under leaf-on conditions in June 2017 covering the entire park. A Riegl LMSQ 680i sensor, operating at a wavelength of 1550 nm, and a beam divergence of 0.5 mrad, was flown at an altitude of 550 m, with a 60% side lap of parallel flight strips. Thus, the average density of points obtained was 30 points/m^2. The positional accuracy of the ALS data was assessed by geometrically checking it with enclosing polygons of flat buildings. This gave an accuracy of 5 cm horizontally and 6 cm vertically. Therefore, the planimetric and vertical displacement between the ALS and TLS data was less than 15 cm and 16 cm, respectively. We generated the DTM of the study area with a resolution of 1.0 m based on the classified ground points provided by the vendor. The height of the aboveground ALS points was then normalized with the obtained DTM.

2.4. Estimation of visibility using TLS

In this study, we focused on the visibility in the understory whose upper height boundary was defined as 2.0 m. Firstly, we applied the TLS-based approach proposed by Zong et al. (2021) to generate the 3D viewshed for understory in a field plot from a single viewpoint. A 3D cumulative viewshed was then created by repeatedly calculating the 3D viewsheds from 225 viewpoints, then summing them into a single 3D viewshed. Finally, the visibility of the field plot was calculated from the derived cumulative viewshed.

To determine the optimal plot size for upscaling, we established and tested nine concentric square plots with the side length varying from 5 to 45 m with a step of 5 m and all centered in the middle of the field plot and oriented north–south (Fig. 2). We determined the largest investigated plot size as 45 m, the diameter of the field plots, so that the TLS point cloud density is high enough to accurately estimate visibility.

To generate a single 3D viewshed for each plot, a subset of point clouds from 0 to 2 m above the ground inside the square plot was extracted first. Next, a 3D voxel-based occupancy grid model of each plot, where each voxel was inferred to be either “occupied” or “free”, was established using the TLS point cloud. The side length of the voxel was set to be 0.1 m, as recommended by Zong et al. (2021). An example occupancy grid is shown in the Supplementary Fig. 1. In addition, to avoid sightlines penetrating below the ground in the following sightline tracing procedure, the DTM constructed at each plot was combined with the occupancy grid model. Finally, a set of sightlines were traced within the combined plot scene, with each sightline having two angles: zenith angle (θ) and azimuth angle (φ) (Fig. 3a). All sightlines radiate from the

Table 3
The ALS metrics selected for the prediction of visibility at different plot sizes. The number in the cell is the rank of variable importance in descending order for each plot size.

Plot size (m)	Hp10_can	Hp50_can	Hp70_can	Hp90_can	Hsd_can	Hskew_can	Hkurt_can	P_ground	Hp10_us	Hp50_us	Hp70_us	Hp90_us	NRD	ORD	LPI	P_NRD	P_LPI	Hp99_sd	Hp99_cv	NFC	NFV	VRM	TRI
5													3	2		1							
10	3												1			2							
15	3	5								1			2			4							
20	2	3											4			5			1				
25	6	3								2			1			5			4				
30	3	5									1		6			4			2				
35	1										4		2			3			5				
40	1										3		2			4							5
45	2										1		3						5				4

Metrics selected Yes No

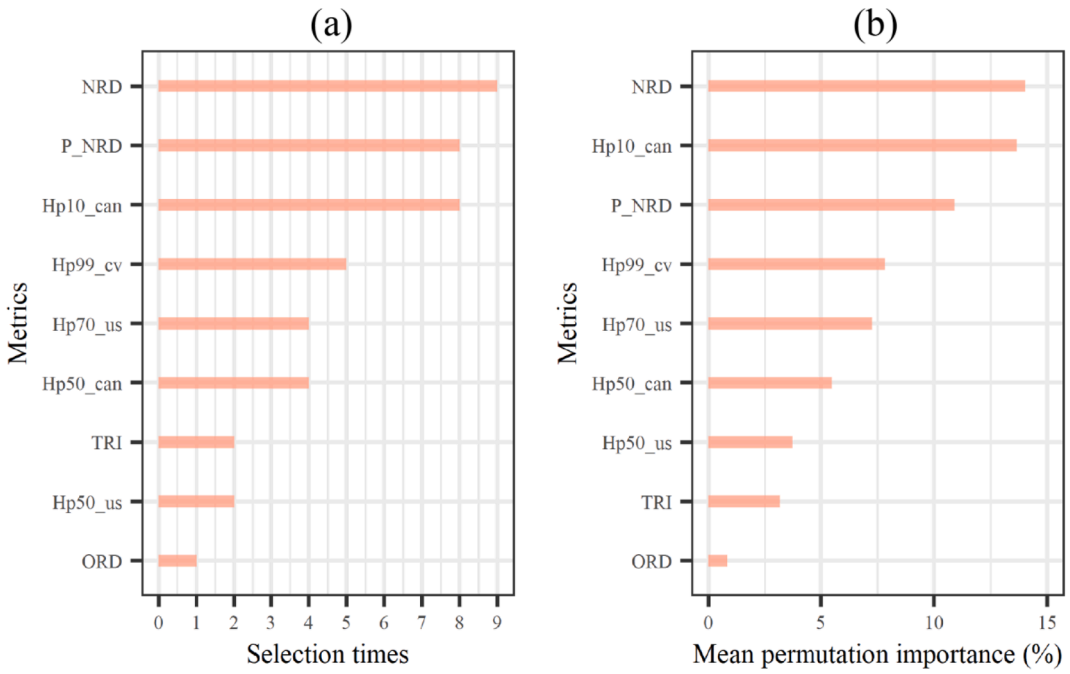

Fig. 5. The overall performance of the selected ALS metrics for prediction of visibility aggregating the results of all final models at different plot sizes. (a) The rank of the times that each metric was selected by all final models, (b) the rank of the mean permutation importance of each metric.

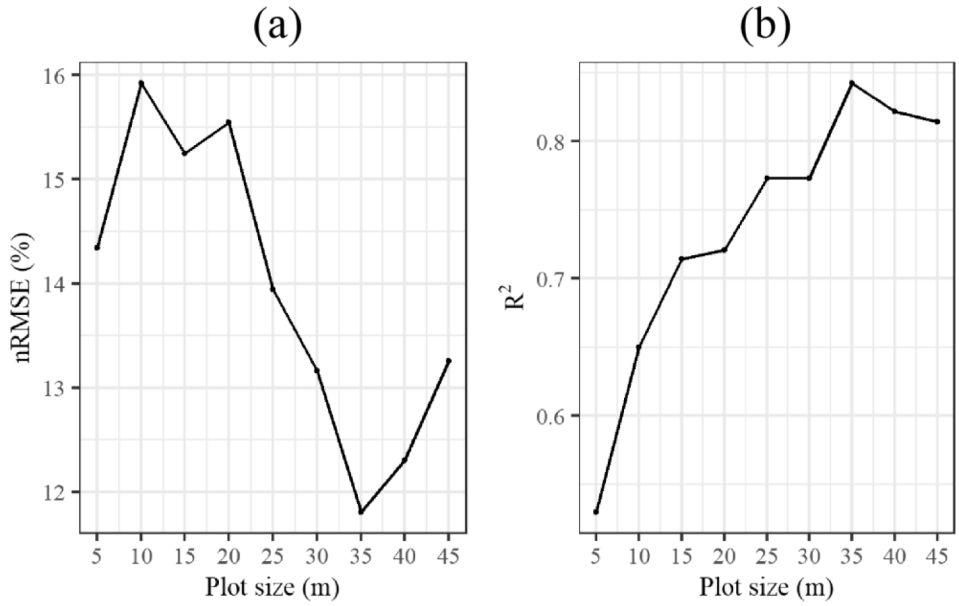

Fig. 6. The relationship between the nRMSE (a) and R^2 (b) of the RF models and the plot sizes.

viewpoint with θ ranging from 0 to 180° as well as φ ranging from 0 to 360° both with an angular step of 0.1°. A sightline is assumed to be blocked by an occupied voxel, a boundary of occupancy grid model, or the DTM, while passing through a free voxel (Fig. 3b). After tracing all sightlines, every voxel in the occupancy grid model will be labeled either "visible" or "invisible" according to whether hit by a sightline, and all visible voxels constitute the 3D viewshed of a plot (Fig. 3c).

The 3D cumulative viewshed tells us how many of the viewpoints from which each voxel can be seen, *i.e.*, their cumulative visibility. The cumulative visibility of each voxel was then normalized according to the total number of viewpoints. The cumulative visibility of the whole plot was calculated as the mean cumulative visibility of all voxels in the plot scene.

For every plot size, 225 (25 × 25) viewpoints were distributed in a grid pattern inside the plot, equally spaced with each other in the northerly and easterly direction at 1.0 m above the ground level (see Supplementary Fig. 2). Our exploratory results showed that the cumulative visibility of the whole plot steadily increased when the number of viewpoints in a single direction was increased from 5 to 25, and then reached an asymptote for denser viewpoints (see Supplementary Fig. 3). Therefore, we consider the differences in cumulative visibility, when the viewpoints are denser than 25 × 25, to be negligible. 225 viewpoints were deployed here to reduce computational cost. Dungan et al. (2018) found a similar result in the case of calculating 2D cumulative viewshed on the DEM.

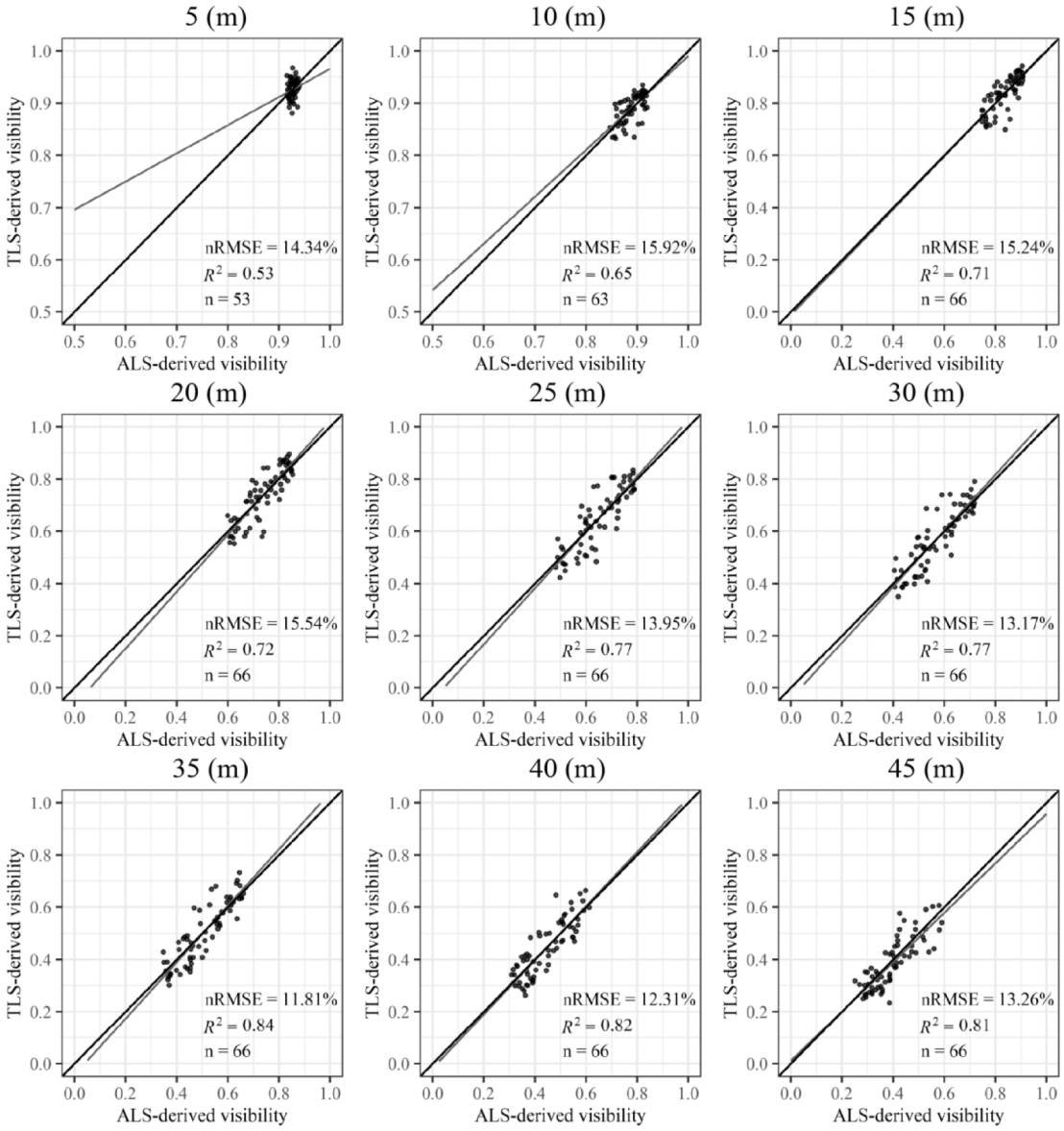

Fig. 7. Relationships between visibility derived from ALS and TLS at various plot sizes. The black dots represent the matched pairs of visibility derived from ALS and TLS for the sample plots. *n* refers to the number of plots involved in the statistical analysis. The blue line is the fitted regression line. The black line indicates the 1:1 relationship. At plot sizes of 5 m and 10 m, some sample plots were removed because some ALS metrics in these plots could not be calculated due to insufficient ALS points. (For interpretation of the references to colour in this figure legend, the reader is referred to the web version of this article.)

2.5. Calculation of ALS metrics

We calculated 23 ALS metrics over each square plot to characterize the canopy, understory, and topographical conditions, using different plot sizes (Table 2). Previous research has shown that many of these metrics are valuable in predicting a variety of understory attributes and can be transferred to similar forest ecosystems. All echoes from each pulse (*e.g.*, single, first, and last) were used to calculate the ALS metrics using the lidR (Roussel et al., 2020), R package for LiDAR data processing.

Percentiles of laser pulse height distribution are the most widely used ALS metrics for forest structure characterization (Lefsky et al., 1999; Naesset, 1997). We calculated the height percentile (HP) of pulse returns at 5% intervals from Hp5 to Hp95 in a plot for canopy and understory separately. Aboveground returns below 2.0 m were classified as understory hits, while those above 2.0 m were classified as canopy hits. Due to a high correlation among these height percentiles, we only selected the Hp10, Hp50, Hp70, and Hp90 percentiles for statistical modeling.

Overall relative point density (ORD) and normalized relative point density (NRD) are associated with understory vegetation density (Campbell et al., 2018). The laser penetration index (LPI) is well correlated with the leaf area index (Peduzzi et al., 2012). In a given area, ORD, NRD, and LPI are defined in the following way, respectively:

$$\mathrm{ORD} = \frac{n_{us}}{n_{total}} \tag{1}$$

$$\mathrm{NRD} = \frac{n_{us}}{n_{us} + n_{ground}} \tag{2}$$

$$\mathrm{LPI} = \frac{n_{us} + n_{ground}}{n_{total}} \tag{3}$$

where n_{us} (understory points) is the number of non-ground returns with height < 2.0 m, n_{ground} (ground points) is the number of ground returns and n_{total} (total points) is the number of returns from the ground level

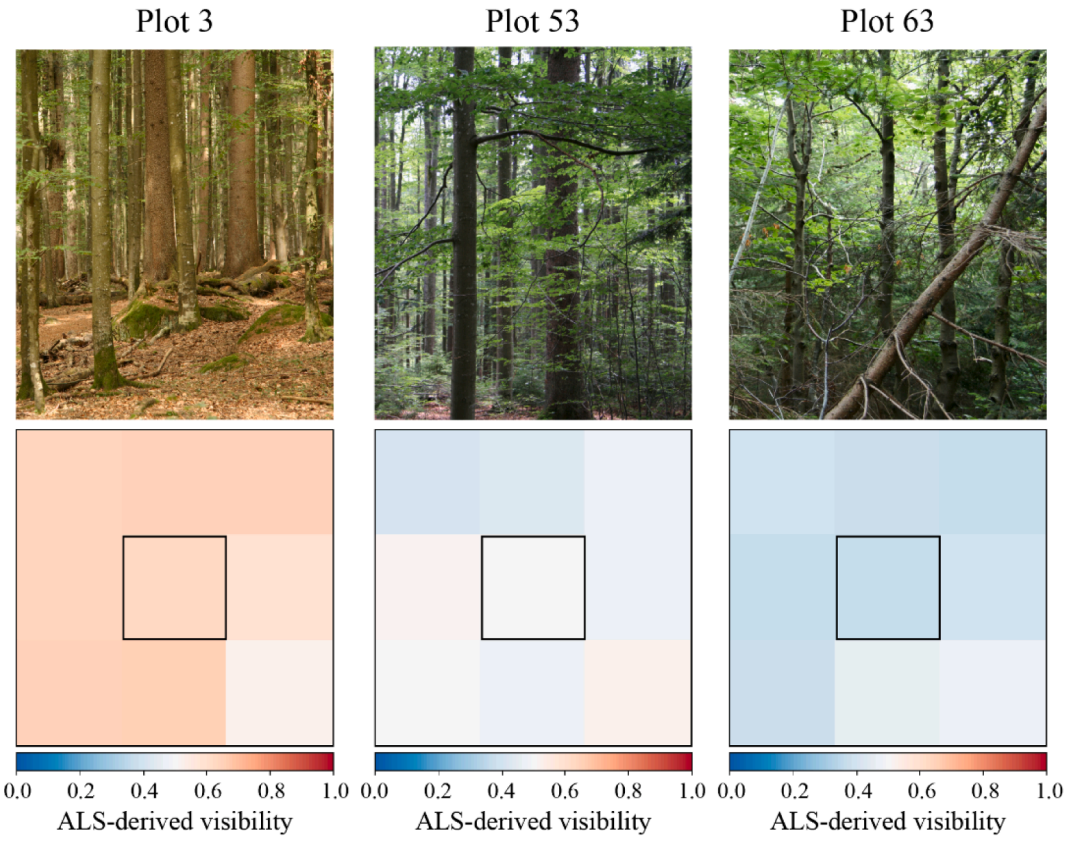

Fig. 8. The field photographs of three sample plots (*i.e.*, plots ID 3, 53, and 63), and its corresponding visibility derived from ALS at a plot size of 35 m (highlighted with a black square). The visibility of its surrounding eight plots was also shown. The photographs were taken at the center of the three plots that represent low, medium, and high levels of understory cover, respectively.

(height = 0 m) to the height of the highest point.

Besides the metrics derived from the vertical distribution of ALS returns, we have calculated several horizontal metrics that attempt to capture the spatial heterogeneity of the understory vegetation relative to the planimetric coordinates. The metric P_NRD is an extension of NRD. We first partitioned the square plot into a square grid, measuring 1 × 1 m. For each such grid cell, the NRD was calculated. The understory vegetation for such a grid cell is arbitrarily assumed to be present if its NRD is more than 10%. Then, P_NRD was calculated as the proportion of such "understory present" grid cells. As similar to P_NRD, P_LPI was calculated as the proportion of grid cells whose LPI is more than 5% and therefore is assumed to be "adequate" regarding the light penetration. For the same grid, we calculated the 99th percentile height of the understory returns for each grid cell and their variation: standard deviation of the Hp99 (Hp99_sd) and coefficient of variation of the Hp99 (Hp99_cv). These two measures mainly characterize the evenness of the understory height over the plot (Gopalakrishnan et al., 2018). The number of filled columns (NFC) and the number of filled voxels (NFV) are calculated based on the voxelization of the ALS point cloud (Crespo-Peremarch et al., 2018). We voxelized the understory hits in a plot using a 1 × 1 × 0.2 m (x × y × z) voxel size to have minimal empty voxels and thus reduce accuracy loss. The horizontal dimension was determined according to the size of the laser footprint and the density of ALS points, where the vertical size was based on the temporal spacing of the sample (*i.e.*, 0.2 m). A voxel containing at least 4 points was defined as filled, and a filled column was required to have at least one filled voxel. NFC is equal to the proportion of the filled voxel columns in the understory, and NFV is calculated as the proportion of the filled voxels in the understory.

We additionally calculated the topographic metrics including vector ruggedness measures (VRM) (Sappington et al., 2007) and terrain ruggedness index (TRI) (Riley et al., 1999) from the ALS-derived DTM to take into account the visual obstruction of the local terrain.

2.6. Random forest algorithm

Random Forest (RF) is a widely used machine learning algorithm that is very effective in classifying and regressing (Breiman, 2001). We used the RF algorithm implemented in the R package "randomForest" (Liaw and Wiener, 2002) to regress the TLS-derived visibility on ALS metrics and to evaluate the performance of the candidate metrics as well as select the most explanatory metrics at different plot sizes. We set up the RF parameter "Ntree" (*i.e.*, number of trees grown) as 500 and parameter "Mtry" (*i.e.*, number of predictors sampled for splitting at each node) as one-third of the number of predictors.

2.6.1. Model performance assessment

As each tree in the RF model is grown from a bootstrap sample of the data, the data left out of the bootstrap sample, the "out-of-bag" (OOB) data, can be used as a test set for that tree. However, OOB error may give an optimistic assessment of the performance of the RF model as discussed by Breiman (2001), therefore we used an external 10-fold cross-validation (CV) procedure replicated by five times to get an averaged coefficient of determination (R^2) and normalized root mean square error (nRMSE; *i.e.*, RMSE divided by the range of the observed values).

2.6.2. Variable importance

In the RF framework, the performance of variables is measured by the variable importance which is crucial not only for variable selection but also for model interpretation (Genuer et al., 2010). The most frequently used variable importance score is the permutation importance which was also used in this study. The permutation importance quantifies the increase in the average OOB error of a tree in the forest

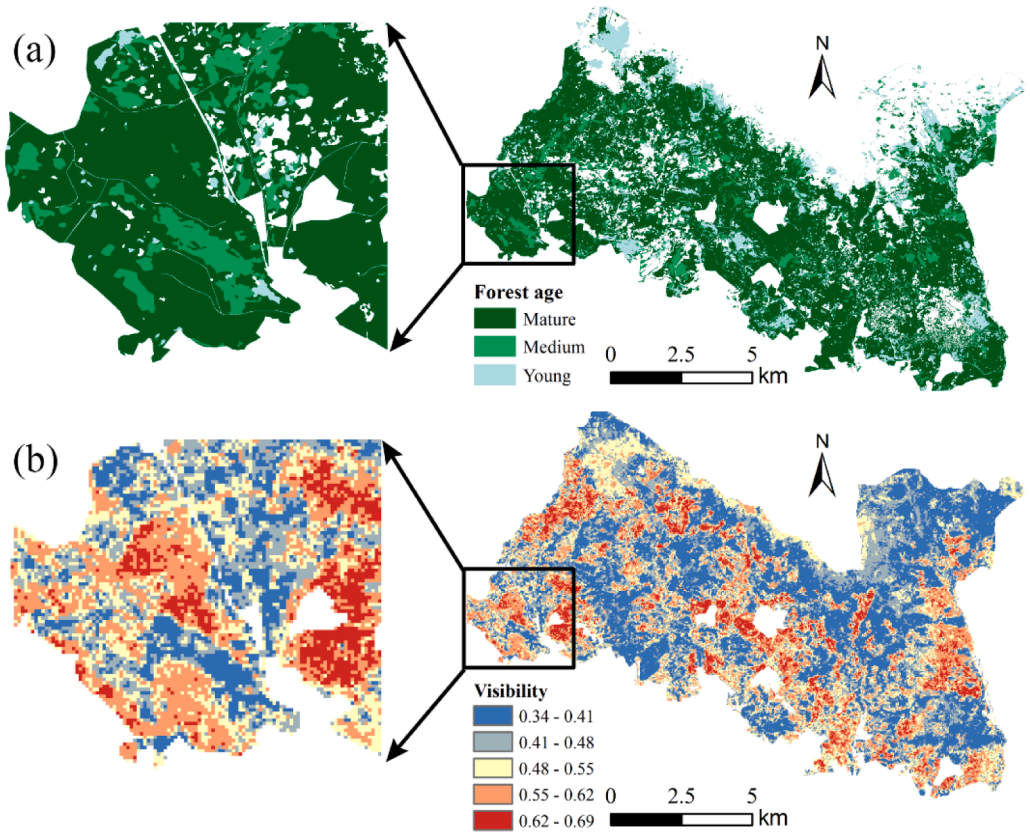

Fig. 9. Maps of the southern part of the Bavarian Forest National Park showing (a) the age of forest stands (Silveyra et al., 2018) and (b) the fine-scale visibility across forest landscapes generated in this study using ALS data.

Table 4
Summary of visibility statistics on various forest age groups.

Forest age	Mature			Medium			Young		
	Coniferous	Deciduous	Mixed	Coniferous	Deciduous	Mixed	Coniferous	Deciduous	Mixed
Mean visibility	0.507	0.495	0.523	0.449	0.427	0.425	0.410	0.386	0.412
Standard deviation	0.073	0.099	0.086	0.076	0.082	0.080	0.044	0.030	0.051
Mean of all	0.508			0.434			0.402		

when the observed values of this variable are randomly permuted in the OOB data.

2.6.3. Variable selection

We applied a modified variable selection method suggested by Genuer et al. (2010). The OOB error in their method was replaced by the R^2 and nRMSE for model performance assessment. By contrast, the variable importance was recalculated repeatedly as the variables were eliminated by a recursive backward procedure, as recommended by Gregorutti et al. (2017). The constituent three main steps of the method were wrapped into the five-time 10-fold CV procedure separately. We aggregated results from all 10-fold CV partitions and computed the mean R^2, nRMSE, and permutation importance at each step.

2.6.4. Metric performance assessment

The performance of a selected metric in the final model for predicting visibility at a given plot size was measured by the mean permutation importance aggregated from all five-time 10-fold CV results. The overall performance of a selected metric was evaluated by the aggregated results from all final models at all plot sizes. We used the times that a metric was selected by all final models to measure its contributing consistency and averaged the permutation importance values of a metric in all final models to measure its contributing significance. If a metric was not selected in the final model at a plot size, its permutation importance was treated as zero.

2.7. Mapping visibility using ALS data

After the statistical comparison, the most accurate RF model, as well as the corresponding optimal plot size and ALS metrics, were identified. We extracted the identified ALS metrics with the optimal plot size and used them as the input of the calibrated optimal RF model to generate a contiguous visibility map of the whole study area.

3. Results

3.1. Estimation of visibility by TLS

As evidenced by Fig. 4, the mean visibility of the plots estimated by TLS steadily decreased from 0.93 to 0.39 with the increase of the plot size from 5 m to 45 m, while the standard deviation increased from 0.02 to 0.12 when the plot size increased from 5 m to 35 m and declined to 0.10 at larger plot size of 45 m.

3.2. Performance of ALS metrics in predicting visibility

Table 3 presents the ALS metrics selected for the prediction of visibility in the final RF model at each plot size and their ranking in variable importance. It demonstrates that the selected ALS metrics and their rankings vary according to the size of the plot. Fig. 5 shows the rank of the metrics in terms of the times that they were selected by all final models (a) and the mean permutation importance (b). The most frequently used metrics in the RF models included, in the descending order of frequency, NRD, P_NRD, Hp10_can, Hp99_cv, Hp70_us, Hp50_can, TRI, Hp50_us, and ORD, while other metrics were not selected by any model. NRD, P_NRD, and Hp10_can consistently appeared as the top three metrics that were mostly selected and provided the most significant contribution at different plot sizes.

3.3. The optimal plot size

As depicted in Fig. 6, the most accurate model for predicting visibility was developed with a plot size of 35 m, with an R^2 of 0.84 and an nRMSE of 11.81%. The nRMSE significantly decreased from 15.92% to 11.81% when the plot size increased from 10 m to 35 m. Further increasing the plot size to 45 m resulted in an increase in nRMSE to 13.25%. The R^2 showed an inverse trend, significantly rising from 0.53 to 0.84 at 35 m, before declining slightly to 0.81 at larger plot sizes. The specific correlation between ALS-derived visibility and TLS-derived visibility for each plot size is shown in Fig. 7. It showed that there was a good agreement between the visibility derived from ALS and TLS with an R^2 ranging from 0.53 to 0.84 and a normalized RMSE varying from 15.92% to 11.81% at various plot sizes.

Fig. 8 shows the field photographs of three sample plots and the corresponding visibility derived from ALS. These three representative plots (*i.e.*, plots ID 3, 53, and 63) demonstrate low, medium, and high understory cover levels, respectively. As depicted in Fig. 8, denser understory vegetation led to lower visibility.

3.4. Mapping visibility using ALS data

Fig. 9b shows the contiguous map of the visibility of the whole study area, which was produced with the optimal plot size of 35 m. Besides, we extracted the visibility of mature, medium, and young forests using the land cover map supplied by the park (Silveyra et al., 2018) and compared the visibility map to the forest age map (Fig. 9a). The spatial variation in visibility concurred with the distribution of mature, medium, and young forests. Overall, visibility decreased with increasing forest age and was particularly high in mature forests (Table 4).

4. Discussion

This study set out to evaluate the applicability of ALS for the estimation of fine-scale visibility in a temperate forest ecosystem. Our findings demonstrate that the fine-scale visibility in forests could be accurately predicted from structural metrics derived from ALS data, with an R^2 ranging from 0.53 to 0.84 and an nRMSE varying from 15.92% to 11.81% at various plot sizes; while the highest accuracy was achieved at a plot size of 35 m.

We found the mean visibility of the plots derived from the TLS decreased with the increase of the plot size and its standard deviation showed an inverse U-shaped trend with regard to the increasing plot size, with the highest standard deviation at 35 m. The decrease in mean visibility is a result of increased visual obstructions in the sightline. The low variance with the small plots is due to the fact that most parts of a target in forest plots are visible at a very close distance. In contrast, a target at a far distance is heavily covered by vegetation, reducing the variance between the different plots. Therefore, there is an intermediate distance at which the highest variance between the different plots is obtained, as also suggested by Nudds (1977) and Murgoitio et al. (2014).

Our results demonstrated that eight ALS metrics, including NRD, P_NRD, Hp10_can, Hp99_cv, Hp70_us, Hp50_can, TRI, and Hp50_us significantly contributed to higher accuracy for predicting fine-scale visibility under the leaf-on condition in forests, with NRD, P_NRD, and Hp10_can being the most important three metrics. These metrics can be categorized into four groups: the metrics characterizing vertical canopy structure including Hp10_can and Hp50_can; the metrics characterizing vertical understory structure including NRD, Hp70_us, and Hp50_us; the metrics characterizing horizontal understory structure including P_NRD and Hp99_cv; and the topographic metrics characterizing terrain ruggedness including TRI. As similar to the prediction of other understory attributes such as fractional cover and density (Crespo-Peremarch et al., 2018), the metrics with regard to canopy conditions are also influential for the prediction of fine-scale visibility. We found that NRD had the most consistent and significant contribution to the accuracy of fine-scale visibility predictions, which implies that fine-scale visibility is highly related to vegetation density in the understory. Our results demonstrate that the metrics that can consider the horizontal understory heterogeneity like P_NRD and Hp99_cv are useful to enhance the description of plant spatial distributions and, consequently, predictions of stand attributes. TRI started to make a difference in predicting fine-scale visibility at large plot sizes. This is because the local terrain within the extent of the small plots is “smooth”, and thus the visual obstruction that results from terrain roughness is small. However, the topographic effect should be carefully checked and is expected to come into play at a relatively small plot size when such studies are carried out in very rough areas.

Overall, our results showed the high performance of ALS data for predicting fine-scale visibility, with the best accuracy at the plot size of 35 m. As our results showed, the variance of the TLS-derived visibility was highest at the optimal plot size of 35 m. As we have revealed, the discrimination of visibility among different plots will be reduced when the plot size is too small or large, and thus the accuracy of the prediction will be lower, particularly with the plot size of 5 or 10 m in this study. The increase in visibility in forest plots with the increase of the plot size depends on the vegetation density. A target will disappear more rapidly from the visual field when it moves from a closer to further distance in a dense forest. It thus implies that the optimum size of the plot is linked to the density of vegetation in the forest. Specifically, the optimal plot size is expected to be smaller in a denser forest (*e.g.*, a tropical forest).

Compared to the accuracy at small plot sizes, Murgoitio et al. (2014) achieved similar results with R^2 values of 0.68 and 0.67 at 5 m and 10 m distance respectively when they regressed ALS-derived trunk and canopy area on the TLS-derived visibility in three predefined directions in a lodgepole pine ecosystem. However, the R^2 decreased steadily to 0.17 when the sightline length increased to 45 m, which is different from the pattern in our study. The reason seems that the TLS data were collected at only one position in their study, which caused a low point density far away from the TLS sensor, and in turn limited the ability of TLS to characterize vegetation structure for visibility modeling. Hence, a multiple TLS scan is needed to estimate fine-scale visibility in forests as suggested by Zong et al. (2021), especially in dense forest plots. Additionally, they found the relationship between ALS-derived trunk as well as canopy area and reference visibility measured by the photography-based method was found to be weak, and they attributed this phenomenon to the canopy shadowing limitation of ALS. In their study, the ALS point density was 8.68 points m^{-2}, much lower than the 30 points m^{-2} in this study. This implies that the point density of ALS data has an important influence on their capacity to quantify fine-scale visibility in forests.

The map of fine-scale visibility in the study area showed a spatial variation in accordance with the forest age map. Mature forests had significantly higher visibility than medium and young forests (Table 4). Previous studies have found that there tends to be less shrub and herbaceous vegetation in old-growth forests than in young forests due to lower resource availability (*e.g.*, light, soil nutrition, and water) (Lindh

et al., 2003; Oliver, 1980; Riegel et al., 1992). As Fig. 8 has shown, visibility decreased when the level of understory cover increased from low to medium, and further to high. Therefore, the relative lack of shrub and herbaceous vegetation results in less visual obstruction and higher visibility in the understory of mature forests than in medium and young forests.

There was a time lag between the collection of the TLS and ALS data in our study. Specifically, ALS data were acquired in June 2017, whereas the TLS data were collected separately in July and August of 2016, 2017, and 2019. Considering that both data were acquired during the summer when the leaves had stopped growing, we expect that the change in the vegetation structure of the understory will be minimal.

The continuous fine-scale visibility map derived by our method can be represented as a layer to model the spatial behavior of animals. It has potential when integrated with remotely collected animal location data, allowing us to better understand the factors that influence animal movement patterns and habitat selection. In previous such studies, the visibility of the animals' habitat is often quantified by surrogate attributes, such as land cover type and canopy cover and height (Filla et al., 2017; Hill et al., 2004; Johnson et al., 2000). However, these attributes are not a physical measure of real visibility. Moreover, proxies for visibility cannot account for the effects of the height of animal eyes and their visual acuity determining the distance at which an animal can detect objects with sufficient resolution to inform behavioral decisions. Using our method, the height of the viewpoints can be determined according to the eye height of the animal of interest and the visual acuity can also be considered for determining the grain size of upscaling.

5. Conclusion

In this study, we evaluated the applicability of ALS data to quantify fine-scale visibility at the landscape level in a mixed temperate forest. Specifically, we examined the ability of 23 commonly used metrics derived from ALS data under the leaf-on condition to characterize the fine-scale visibility. We also evaluated the effect of field plot size on the accuracy of the fine-scale visibility estimate. We verified the estimated visibility from the ALS using TLS-derived visibility. Based on the results we conclude that ALS-derived structural metrics accurately predict fine-scale visibility in the mixed temperate forest. The optimum plot size was 35 × 35 m. ALS offers an efficient and accurate way to upscale 3D visibility in forests to a landscape and regional level – an application previously limited to the plot level (*e.g.*, approximately 30 × 30 m) using TLS data. As this study was conducted in a central European mixed temperate forest, further research is necessary to test whether similar accuracies may be obtained in other forest ecosystems with higher canopy density and tree species mixes, using ALS data.

CRediT authorship contribution statement

Xin Zong: Funding acquisition, Conceptualization, Methodology, Investigation, Data curation, Formal analysis, Validation, Visualization, Writing - original draft. **Tiejun Wang:** Conceptualization, Methodology, Investigation, Validation, Supervision, Resources, Writing - review & editing. **Andrew K. Skidmore:** Funding acquisition, Conceptualization, Methodology, Validation, Supervision, Resources, Project administration, Writing - review & editing. **Marco Heurich:** Validation, Supervision, Resources, Writing - review & editing.

Declaration of Competing Interest

The authors declare that they have no known competing financial interests or personal relationships that could have appeared to influence the work reported in this paper.

Acknowledgments

The work of the first author was sponsored by the China Scholarship Council (grant number 201704910852). The authors are thankful for the support of the European Research Council (European Commission BIOSPACE—Monitoring Biodiversity from Space project; grant agreement 834709, H2020-EU.1.1.), and the "Data Pool Initiative" of the Bohemian forest ecosystem.

Appendix A. Supplementary data

Supplementary data to this article can be found online at https://doi.org/10.1016/j.jag.2021.102478.

References

Bao, S., Xiao, N., Lai, Z., Zhang, H., Kim, C., 2015. Optimizing watchtower locations for forest fire monitoring using location models. Fire Saf. J. 71, 100–109.
Breiman, L., 2001. Random Forests. Machine Learning 45, 5–32.
Cailleret, M., Heurich, M., Bugmann, H., 2014. Reduction in browsing intensity may not compensate climate change effects on tree species composition in the Bavarian Forest National Park. For. Ecol. Manage. 328, 179–192.
Caldwell, D.R., Ehlen, J., Harmon, R.S., 2005. Studies in military geography and geology. Kluwer Academic Publishers, Dordrecht.
Campbell, M.J., Dennison, P.E., Hudak, A.T., Parham, L.M., Butler, B.W., 2018. Quantifying understory vegetation density using small-footprint airborne lidar. Remote Sens. Environ. 215, 330–342.
Chamberlain, B.C., Meitner, M.J., Ballinger, R., 2015. Applications of visual magnitude in forest planning: A case study. The Forestry Chronicle 91, 417–425.
Crespo-Peremarch, P., Tompalski, P., Coops, N.C., Ruiz, L.Á., 2018. Characterizing understory vegetation in Mediterranean forests using full-waveform airborne laser scanning data. Remote Sens. Environ. 217, 400–413.
Dassot, M., Constant, T., Fournier, M., 2011. The use of terrestrial LiDAR technology in forest science: application fields, benefits and challenges. Annals of Forest Science 68, 959–974.
Domingo-Santos, J.M., de Villarán, R.F., Rapp-Arrarás, Í., de Provens, E.C.-P., 2011. The visual exposure in forest and rural landscapes: An algorithm and a GIS tool. Landscape Urban Plann. 101, 52–58.
Drummond, R.R., 1956. Visibility in some forest stands of the United States. Quartermaster Research & Development Center, Environmental Protection ….
Dungan, K.A., White, D., Déderix, S., Mills, B.J., Safi, K., 2018. A total viewshed approach to local visibility in the Chaco World. Antiquity 92, 905–921.
Dupke, C., Bonenfant, C., Reineking, B., Hable, R., Zeppenfeld, T., Ewald, M., Heurich, M., 2017. Habitat selection by a large herbivore at multiple spatial and temporal scales is primarily governed by food resources. Ecography 40, 1014–1027.
Filla, M., Premier, J., Magg, N., Dupke, C., Khorozyan, I., Waltert, M., Bufka, L., Heurich, M., 2017. Habitat selection by Eurasian lynx (Lynx lynx) is primarily driven by avoidance of human activity during day and prey availability during night. Ecol. Evol. 7, 6367–6381.
Genuer, R., Poggi, J.-M., Tuleau-Malot, C., 2010. Variable selection using random forests. Pattern Recogn. Lett. 31, 2225–2236.
Göltaş, M., Demirel, T., Çağlayan, İ., 2017. Visibility Analysis of Fire Watchtowers Using GIS; A Case Study in Dalaman State Forest Enterprise. European Journal of Forest Engineering 3, 66–71.
Gopalakrishnan, R., Thomas, V.A., Wynne, R.H., Coulston, J.W., Fox, T.R., 2018. Shrub detection using disparate airborne laser scanning acquisitions over varied forest cover types. Int. J. Remote Sens. 39, 1220–1242.
Gregorutti, B., Michel, B., Saint-Pierre, P., 2017. Correlation and variable importance in random forests. Statistics and Computing 27, 659–678.
Griffith, B., Youtie, B.A., 1988. Two Devices for Estimating Foliage Density and Deer Hiding Cover. Wildl. Soc. Bull. 1973–2006 (16), 206–210.
Guth, P.L., 2009. Incorporating vegetation in viewshed and line-of-sight algorithms. 2009: DIGITAL MAPPING: From Elevation to Information. ASPRS/Mapps 2009 Specialty Conference, San Antonio, Texas.
Higgins, K.F., Oldemeyer, J., Jenkins, K., Clambey, G., Harlow, R., 1996. Vegetation sampling and measurement. Research and management techniques for wildlife and habitats 5, 567–591.
Hill, R.A., Hinsley, S.A., Gaveau, D.L.A., Bellamy, P.E., 2004. Cover: Predicting habitat quality for Great Tits (*Parus major*) with airborne laser scanning data. Int. J. Remote Sens. 25 (22), 4851–4855.
Johnson, B.K., Kern, J.W., Wisdom, M.J., Findholt, S.L., Kie, J.G., 2000. Resource selection and spatial separation of mule deer and elk during spring. J. Wildl. Manag. 685–697.
Lecigne, B., Eitel, J.U., Rachlow, J.L., 2020. viewshed3d: An r package for quantifying 3D visibility using terrestrial lidar data. Methods Ecol. Evol. 11, 733–738.
Lefsky, M.A., Harding, D., Cohen, W., Parker, G., Shugart, H., 1999. Surface lidar remote sensing of basal area and biomass in deciduous forests of eastern Maryland, USA. Remote Sens. Environ. 67, 83–98.
Liaw, A., Wiener, M., 2002. Classification and regression by randomForest. R news 2, 18–22.

Lindh, B.C., Gray, A.N., Spies, T.A., 2003. Responses of herbs and shrubs to reduced root competition under canopies and in gaps: a trenching experiment in old-growth Douglas-fir forests. Can. J. For. Res. 33, 2052–2057.
Loarie, S.R., Tambling, C.J., Asner, G.P., 2013. Lion hunting behaviour and vegetation structure in an African savanna. Anim. Behav. 85, 899–906.
Morrison, L.W., 2016. Observer error in vegetation surveys: a review. Journal of Plant Ecology 9, 367–379.
Murgoitio, J., Shrestha, R., Glenn, N., Spaete, L., 2014. Airborne LiDAR and terrestrial laser scanning derived vegetation obstruction factors for visibility models. Transactions in GIS 18, 147–160.
Murgoitio, J.J., Shrestha, R., Glenn, N.F., Spaete, L.P., 2013. Improved visibility calculations with tree trunk obstruction modeling from aerial LiDAR. International Journal of Geographical Information Science 27, 1865–1883.
Næsset, E., 2002. Predicting forest stand characteristics with airborne scanning laser using a practical two-stage procedure and field data. Remote Sens. Environ. 80, 88–99.
Naesset, E., 1997. Determination of mean tree height of forest stands using airborne laser scanner data. ISPRS J. Photogramm. Remote Sens. 52, 49–56.
Nudds, T.D., 1977. Quantifying the vegetative structure of wildlife cover. Wildl. Soc. Bull. 5, 113–117.
Oliver, C.D., 1980. Forest development in North America following major disturbances. For. Ecol. Manage. 3, 153–168.
Peduzzi, A., Wynne, R.H., Fox, T.R., Nelson, R.F., Thomas, V.A., 2012. Estimating leaf area index in intensively managed pine plantations using airborne laser scanner data. For. Ecol. Manage. 270, 54–65.
Pyysalo, U., Oksanen, J., Sarjakoski, T., 2009. Viewshed analysis and visualization of landscape voxel models, 24th international cartographic conference. Santiago, Chile.
Riegel, G.M., Miller, R.F., Krueger, W.C., 1992. Competition for resources between understory vegetation and overstory Pinus ponderosa in northeastern Oregon. Ecol. Appl. 2, 71–85.
Riley, S.J., DeGloria, S.D., Elliot, R., 1999. Index that quantifies topographic heterogeneity. Intermountain Journal of Sciences 5, 23–27.
Roussel, J.R., Auty, D., Coops, N.C., Tompalski, P., Goodbody, T.R., Meador, A.S., Bourdon, J.F., de Boissieu, F., Achim, A., 2020. lidR: An R package for analysis of Airborne Laser Scanning (ALS) data. Remote Sens. Environ. 251, 112061.
Sappington, J.M., Longshore, K.M., Thompson, D.B., 2007. Quantifying landscape ruggedness for animal habitat analysis: a case study using bighorn sheep in the Mojave Desert. J. Wildl. Manag. 71, 1419–1426.
Silveyra, G., Ramiro, Latifi, H., Weinacker, H., Dees, M., Koch, B., Heurich, M., 2018. Integrating LiDAR and high-resolution imagery for object-based mapping of forest habitats in a heterogeneous temperate forest landscape. International Journal of Remote Sensing 39, 8859-8884.
Vukomanovic, J., Singh, K.K., Petrasova, A., Vogler, J.B., 2018. Not seeing the forest for the trees: Modeling exurban viewscapes with LiDAR. Landscape Urban Plann. 170, 169–176.
Wheatley, D., 1995. Cumulative viewshed analysis: a GIS-based method for investigating intervisibility, and its archaeological application. Archaeology and geographical information systems: a European perspective 171–185.
Winnard, A.L., Di Stefano, J., Coulson, G., 2013. Habitat use of a critically-endangered species in a predator-free but degraded reserve in Australia. Wildlife Biology 19, 429–438.
Zong, X., Wang, T., Skidmore, A.K., Heurich, M., 2021. The impact of voxel size, forest type, and understory cover on visibility estimation in forests using terrestrial laser scanning. GIScience & Remote Sensing 1–17.